MADRID
inter.noise 2019
June 16 - 19
NOISE CONTROL FOR A BETTER ENVIRONMENT

Experimental and Numerical Aeroacoustic Analyses of a Large-scale Flap Side-edge Model

Acevedo-Giraldo, Daniel[1]., Botero-Bolívar, Laura., L. Pereira, Lourenço T. and Catalano, Fernando M.
São Carlos School of Engineering, University of São Paulo (EESC-USP)
Av. Trab. São Carlense 400, São Carlos - SP, Brazil

Reis, Danillo C.[2] and C. Coelho, Eduardo L.
Embraer
Av. Brigadeiro Faria Lima 2170, São José dos Campos - SP, Brazil

ABSTRACT

In this research, the relationship between the parameters of a large-scale flap model and the physics responsible for flap side-edge noise generation, one of the most dominant sources of the airframe noise was investigated in experimental and computational tests. Flow-field measurements were taken according to phased microphone array techniques toward a deeper understanding of flap side-edge noise sources and their correlations to unsteady vorticity fluctuations. Conventional beamforming, CLEAN-SC and DAMAS methodologies provided far-field acoustic spectra estimations and noise source mapping, and numerical investigations were conducted by the commercial version of PowerFLOW 5.3®. The model used for the tests consists of an unswept isolated flap element with representative tip details present in a conventional medium-range transport aircraft. Different side-edge devices were assessed toward reductions in airframe noise. A perforated side-edge treatment was also applied to the flap side-edge. Aeroacoustic tests were conducted in the LAE-1 closed circuit wind tunnel with a closed working section at the São Carlos School of Engineering - University of São Paulo (EESC-USP) at up to 40 m/s flow speeds and the results provided specific information about the aeroacoustic characterization of the dominant acoustic source mechanisms of the flap model.

Keywords: Airframe noise, Flap noise, Flap side-edge, Experimental aeroacoustics and Numerical aeroacoustics
I-INCE Classification of Subject Number: 10
http://i-ince.org/files/data/classification.pdf

[1] daniel.acevedogi@usp.br
[2] danillo.reis@embraer.com.br

1. INTRODUCTION

Aircraft noise is defined as the noise perceived by an individual on the ground. The total noise is the result of sound radiated by several sources related to an aircraft. The contribution of each source to the overall aircraft noise varies with the phase of flight. The aircraft noise mainly refers to propulsion system noise and airframe noise [1], also known as "Non-propulsive noise of an aircraft in flight" [2].

Engine noise is the major contributor to the overall aircraft noise during take-off, since the engines are set to their maximum power to provide the necessary thrust. The contribution of the airframe noise is more significant during the approach operation, once it becomes equally important as engine noise [3], since the aircraft demands less thrust and the generation of engine noise is reduced. Both high-lift devices (flap and slat) and landing gear are the main sources of overall aircraft noise only during approach and take-off, since all of them are retracted in the cruise phase [4].

The noise generated from flap side-edge is recognized as one of the most effective source of airframe noise [5-8] because of two main noise generation mechanisms described by Rossignol, K., (2013) [9]. The former is a direct interaction between the shear layer unsteadiness and the sharp edge, and the second is the induction of vortex unsteadiness interacting with the surfaces and edges. The pressure differential between the upper and lower surfaces produces an oscillating vortical system, which results in a strong broadband noise. Such a system is characterized by the generation of two separate vortices in the upstream region of the flap, i.e., one at the upper flap side contour and the other at the lower flap side contour [10]. As stated by Molin, N., (2003) [11], in general, any vortical pattern in a flow generates sound as soon as its inertia has been modified, once the corresponding change in the pressure gradients also induces density fluctuations that propagate as sound. At commonly subsonic Mach numbers, sound generation occurs as convected vortical patterns interact with solid surfaces.

According to Reichenberger, J., (2016) [10] and Filippone, A., (2014) [12] flap local flow-field comprises the following noise generation mechanisms described by Rossignol, K., (2013) [9]. The flap side-edge local flow-field noise generation mechanisms are: I. Trailing-edge noise and flow separation at the tip edges. (I.a). The turbulent boundary layer on the pressure side of the flap moves across the lower flap side-edge. This mechanism is present in the entire flap chord region. (I.b). The turbulent boundary layer on the side of the flap moves across and separates at the upper flap side-edge. II. Fluctuations on the side-edge vortex pressure interacting with the flap side surface and upper side-edge. The vortex is fed by shear instabilities from lower side-edge in the mid-chord region. III. Merging of the two vortices. IV. Fluctuations in the merged vortex pressure interacting with the flap suction and the upper side-edge. (IV.a). The merged vortex moves upwards; this mechanism is limited to a small region slightly downstream of the merging location. (IV.b). The vortex breakdown is a noise source. (IV.c). The merged vortex remains close to the upper surface and interacts with the flap suction side and the upper side-edge. (IV.d). The merged vortex passes the trailing-edge and interacts with the trailing-edge corner.

According to Drobietz, R., and Borchers, I., (2006) [13] flap side-edge noise is considered a broadband component. The post-merged vortex interacting with the flap suction side and the trailing edge; and the shear layer originating at the lower ridge of the flap tip produce most of the audible noise. The unstable merged vortex generates noise in low to mid frequencies, whereas the mid- to high-frequency noise is radiated by turbulent shear layer instabilities.

This investigation focuses on noise reduction associated with the flow-field around a detailed flap side-edge, provide a much deeper understanding of the mechanisms

responsible for the flap noise generation on the subject of large-scale flap side-edge noise for the correct quantification of the noise parameters modeled in Reynolds number at take-off and landing conditions. Experimental and numerical aeroacoustic measurements were conducted by a large-scale flap model, with representative tip details present in a conventional commercial aircraft for a better understanding of the airframe noise phenomena around flap side-edge. The relative contribution of each noise source to the overall airframe noise (at first with baseline flap model configuration and then the flap model with different flap side-edge geometries) is shown in the experimental and numerical measurement comparisons results. This research is a continuation of the flap side-edge work presented previously by Acevedo, D. et al., (2018) [14].

2. FLAP MODEL DESIGN

The flap model designed for investigating the phenomena of airframe noise from side-edge was representative of a detailed flap of a conventional commercial aircraft. A 0.70 m chord flap was used for increasing both Strouhal and Reynolds numbers during the tests and the fidelity of results. The unswept model had also 0.70 m span to match the flap side-edge and the microphone array center. The model does not include many components and is composed of fairly-simple shapes, as shown in Figure 1, therefore, it facilitates measurements and the understanding of the main flow phenomena and their relation to noise emission.

The main structure of the wood-aluminium model is composed of ribs and a simplified iron body-pod formed by two spars and a circular-base (end-plate) fixed to a turn-table mounted at the wind-tunnel test section through an iron link and screws that adjust the angle of attack of the turn-table, hence, the flap model. A removable flap side-edge, with the tested geometries and approximately 0.08 m span, was used at the tip of the model to facilitate the reproduction of the model details and the noise-reduction devices tested.

Figure 1. Flap model geometry

Experiments were performed with and without trip. The trip forces transition, eliminating laminar boundary layer effects (low Reynolds number effects). A 12 mm length and 0.1 mm thick trip tape was placed over the complete span-wise length on the suction side of the flap at $x/c = 0.02$ and on its pressure side at $x/c = 0.06$ to ensure the development of fully turbulent boundary layers and avoid a premature separation of the boundary layers at the trailing-edge. The trip positioning not varied during the experiments.

The tests were performed for three main different configurations, i.e., baseline, which represents a common flap side-edge, the seal flap side-edge, which has real details on the flap tip and the new seal flap side-edge, same as the seal tip with a tab. The last two configurations were also tested with a 22% perforated flap side-edge.

3. EXPERIMENTAL SET-UP

3.1 Wind Tunnel Facility

Experiments and analyses were performed at LAE-1 wind tunnel facilities (Figure 2), at the Laboratory of Aerodynamics of the Aeronautical Engineering Department from São Carlos School of Engineering - University of São Paulo (EESC-USP) [15]. The closed circuit wind tunnel is a low-speed facility with a closed test section of 3.00 m length, 1.30 m height and 1.70 m width. It has an eight-blade fan, driven by a 110 HP electric motor with seven straighteners located downstream the fan, and two 54% porosity screens located before the contraction cone for turbulence reduction, which results in impressive turbulence levels lower than 0.25%. Its Maximum design free flow speed is 50 m/s, however, the maximum current free flow speed is 45 m/s due to components endurance and operational safety, according to Santana et al., (2010) [16].

The LAE-1 wind-tunnel was designed originally for automotive tests, however, it has become a multi-task facility used mainly for aeronautical tests. A background noise reduction process for aeroacoustic measurements has been recently implemented due to the stringent aircraft noise regulations for aircraft certification and operations that require aeroacoustic improvements. The noise treatment processes reduced up to 5 dB the background noise and the turbulence level decreased from the original 0.25% to 0.21% [16].

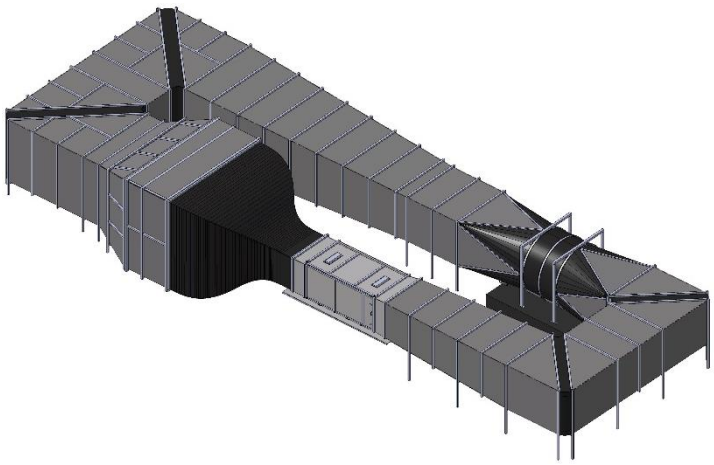

Figure 2. LAE-1 wind tunnel facility 3D view

3.2 Tests Conditions

The LAE-1 wind-tunnel was operated at velocities from 26 to 38 m/s, which correspond to Reynolds numbers based on the chord length of the model from 1.02×10^6 to 1.48×10^6, respectively. The range of Reynolds numbers is given in Table 1. The test flow conditions are the same as those of the wind tunnel location conditions. The atmospheric conditions measured were temperature T = 20 ºC and pressure P = 91.45 KPa, which implied density ρ = 1.067 Kg/m^3, kinematic viscosity $\nu = 1.746 \times 10^{-5}$ m^2/s, dynamic viscosity $\mu = 1.863 \times 10^{-5}$ Pa.s and speed of sound a =337 m/s. The flap model was tested for deflection angles from $\alpha = 20^o$ to 30^o in steps of 2^o.

Table 1 Non-dimensional flow parameters for different tests

U [m/s]	M [-]	Re [-]
26	0.076	1.02 x 10^6
39	0.085	1.14 x 10^6
32	0.094	1.27 x 10^6
35	0.101	1.38 x 10^6
38	0.109	1.48 x 10^6

3.3 Aeroacoustic Measurements

Aeroacoustic measurements were performed in the experimental phase in the model in flyover position through phased array beamforming techniques for providing acoustic source localization and an estimation of the far-field noise spectrum.

3.3.1 Aeroacoustic Transducers

The measurements were taken with an array of 61 microphones flush-mounted on the test section side-wall of the wind tunnel, facing the pressure surface of the flap model for sound pressure acquisition. The G.R.A.S. 46BD microphone set consists of a microphone cartridge with a pressure transducer (40BD) and a preamplifier (26CB) combination, calibrated as one unit. The transducer allows TEDS (Transducer Electrical DataSheet) operation. It provides a flat response for source localization from 4~Hz to 70~kHz (pm 2~dB) frequencies.

The microphone array was designed with a modified and optimized spiral geometry for measurements at a large frequency band [17]. The array was distributed in a 0.85 m diameter region and the flap side-edge was located in the microphone array center, as shown in Figure 3. The center of the turn-table is 0.85 m near the acoustic array. Each microphone was calibrated prior to noise measurements.

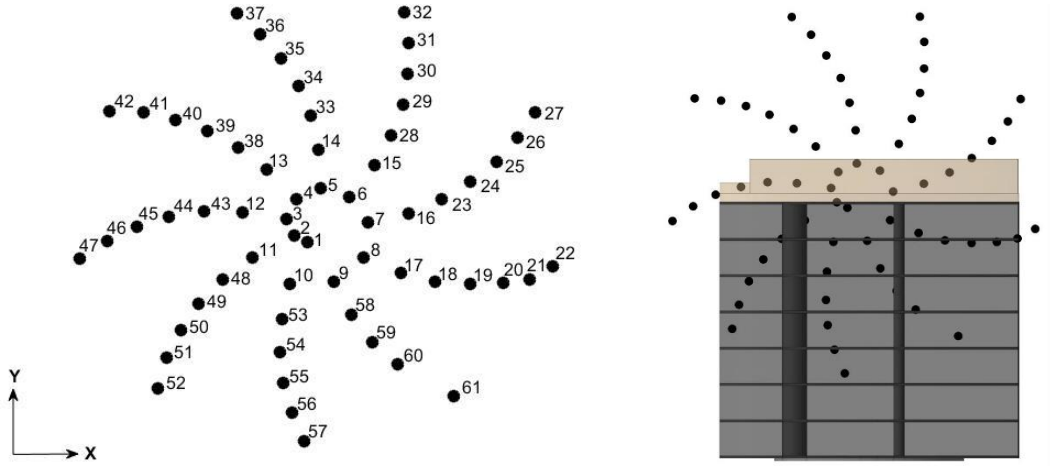

Figure 3. Microphone array position

3.3.2 Acquisition and Calibration

Microphone array acquisition were performed through an IEPE PXI system composed of 4 NI PXIe-4497 boards that hold simultaneously 64 analog inputs of 24 bits resolution and maximum of 204.8 kS/s sample rate. Microphone data is acquired for 20 seconds. PXI is a platform for measurement and automation systems, where the phased array signals captured by the microphones are processed prior to being sent to the computer. The calibration of the microphone array was performed using an NC-74 sound calibrator [18] with 94 dB ± 0.3 dB sound pressure level, 1 kHz ± 2% frequency and 1.0 Pa reference pressure fluctuation for the microphone adapter.

3.4 Data Post-processing

Acoustic measurements were taken in a closed facility and a phased microphone array acquired the data. Two post-processing analyses for aeroacoustic measurements were used. The first provided results of noise spectra in the frequency domain and the second was based on phased array microphones and beamforming techniques to map the location of the noise sources and their intensity. Beamforming calculations were performed by Conventional beamforming [19] and CLEAN-SC [20] methodologies for all data and DAMAS deconvolution [21] methodology for selected cases.

Two Regions of Interest (ROI) were created for the beamforming integration regions. These regions assess the noise contribution measured by each of the different regions of the model. The flyover ROIs (Figure 4) were created for the total model for experimental comparisons and total flap side-edge for numerical comparisons.

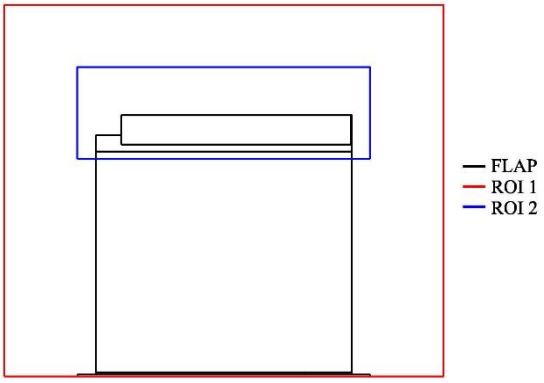

Figure 4. Regions of interest for beamforming calculations. Flap model is shown in black and integration regions are shown in colors.

4. NUMERICAL SET-UP

Numerical simulations were carried out on the commercial software PowerFLOW 5.3 ®, which uses Lattice Boltzmann Method (LBM) as fluid solver and Very Large Eddy Simulations (VLES) based on the κ-ε RNG model as turbulence model. The effects of the unresolved (sub-grid) scale-flow properties on the resolved large scale are exerted via eddy viscosity and turbulent Prandtl numbers and the elements closest to the surface are resolved with the Universal Law of the Wall velocity profile coupled with the wall model pressure gradient extension for determining the local skin fiction. Different from conventional computational fluid dynamic programs that use Navier-Stokes equations, the LBM incorporates the physics of microscopic processes and the fluid is replaced by fraction particles using a distribution function that considers the behavior of a collection of particles a unit [22]. For the far-field analysis PowerFLOW uses the Ffowcs William-Hawking (FW-H) acoustic analogy, which needs measurement of pressure fluctuations in the surface.

The dimensions of the computational domain were 6.50 x 1.70 x 1.30 m for replicating the wind tunnel dimensions. The dimension in the streamwise direction was greater in order to guarantee the fully flow development. Atmospheric conditions used in the simulations were the same as those of the wind tunnel. The velocity inlet was set at 34 m/s with 0.21% turbulence level (wind tunnel turbulence level at 34 m/s according to Santana et al., (2014) [23]) and 1 mm turbulence length scale. The outlet condition was imposed with no pressure gradient and the wind tunnel walls were set as non-friction hard walls. The outermost fluid region was modeled as high viscosity fluid or anechoic layer for the absorption of acoustic waves. The physical discretization was completed with 4.3 x 10^8 elements and the time was discretized into 711594 timesteps (0.4 s in real time).

Simulations taked 48910 CPU hours. The FW-H measurements were taken from a crop in the flap tip, with 1.17c x 0.25c x 0.23c dimensions with 58 kHz sample frequency. Measurements stared after 0.114 s for eliminating transient effects.

5. RESULTS

Apart from the Conventional and CLEAN-SC beamforming analysis for all flap tip geometries, DAMAS methodology was employed for the selected cases. The analysis of the three different beamforming methodologies tested aims to explain the behavior behind methodology procedures, rather than to find the most correct beamforming methodology.

The obtained results for measurements with the three different methodologies at the largest Region of Interest (ROI 1) are shown in Figure 5. The spectra show that broadband noise follows the same shape for all methodologies. Nevertheless, the noise spectra calculated by conventional beamforming and DAMAS methodology preserved the same behavior and showed similar tendencies at low and mid frequencies. CLEAN-SC and DAMAS revealed a higher slope in the high frequency range.

By their own formulations, the conventional beamforming and DAMAS methodology produce a continuum spectrum. The CLEAN-SC concentrates the spectral energy of the coherent noise sources into a single point, which produced pronounced peaks that changed the levels in the spectrum mainly in low frequencies. The following aeroacoustic results were obtained using conventional beamforming considering that the metodology produce results in similar trends to the CLEAN-SC and DAMAS because of the flap side-edge noise was the prominent and dominant noise source during the aeroacoustic measurement.

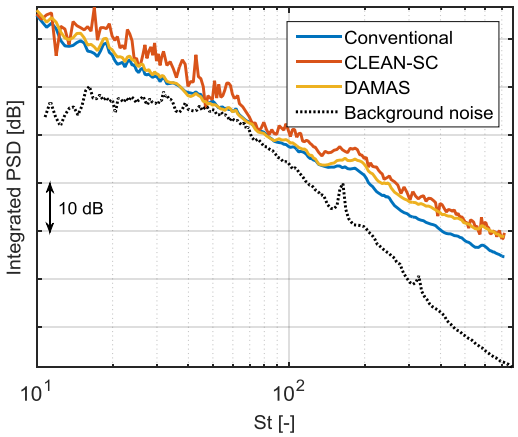

Figure 5. Effect of the beamforming methodology (Conventional, CLEAN-SC and DAMAS) on the seal flap side-edge tip at $\alpha = 26^o$

Far-field acoustic comparisons between numerical and experimental results of the flap model in flyover position are shown in Figure 6. The figures show a level discrepancy of about 8 dB in low and high frequencies that was possibly caused by differences between experimental and numerical post-processing procedures, considering the measurements of microphones in different locations in the wind tunnel and predictions for a single microphone location by the PowerFLOW. In all cases, both spectra present a similar behavior within most of the frequency range, between 50 and 300 Strouhal. Experimental results were affected by the background wind tunnel noise in the low frequency range.

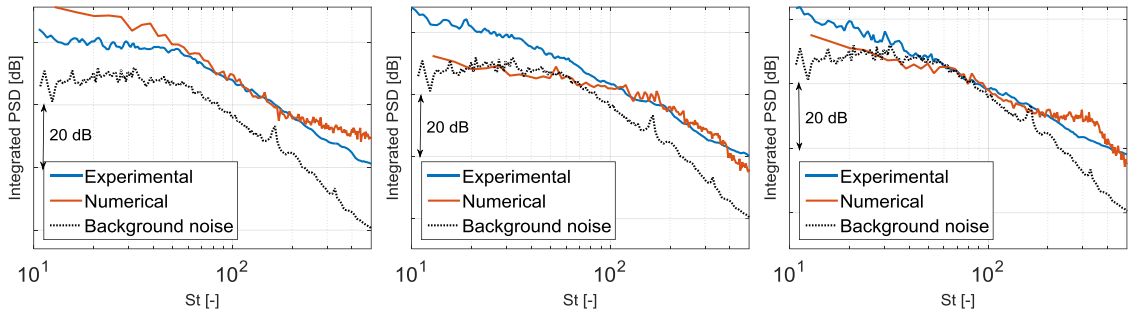

(a) Baseline flap side-edge *(b) Seal flap side-edge* *(c) New seal flap side-edge*

Figure 6. Flyover acoustic spectrum comparison at α = 26o and M = 0.109

The results of the filtered pressure spectrum over the flap side-edge are shown in Figure 7. The numerical simulations reveal how the integrated pressure fluctuations in a range between Strouhal 36.8 - 55.2 are spread over the side-edge, suggesting that the interaction between the pressure side vortex and the side-edge surface plays a major role in noise generation whereas higher Strouhal fluctuations (276.3 – 294.7) are influenced by the shear-layer over the edges of the model. The baseline tip presents the maximum fluctuations from the leading-edge to the half-chord region following the reattachment line of the vortex. Two distinct edges of maximum fluctuations are observed in the seal tip due to the shear-layer interactions with the lower side at the aft-half chord in the leading-edge region and side-edge upper side at the forward half-chord. The results of the filtered pressure spectrum over the new seal tip were similar to those of the seal flap side-edge.

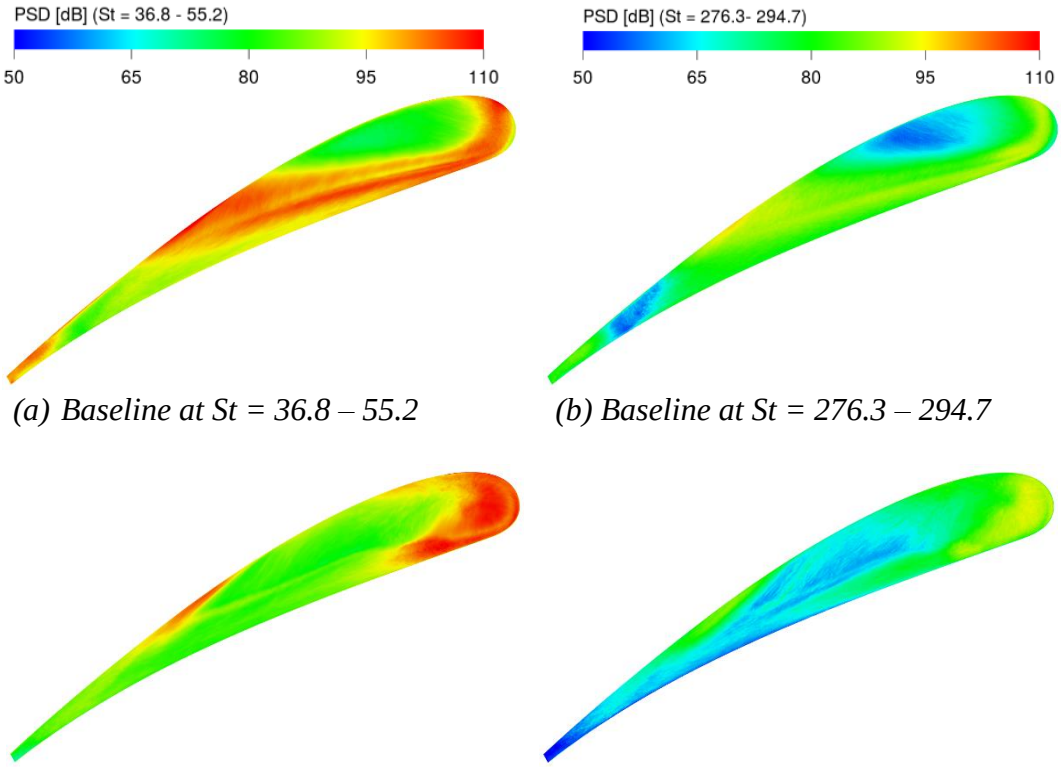

(a) Baseline at St = 36.8 – 55.2 *(b) Baseline at St = 276.3 – 294.7*

(c) Seal at St = 36.8 – 55.2 *(d) Seal at St = 276.3 – 294.7*

Figure 7. Filtered pressure spectrum contour over the flap side-edge at α = 26° and M = 0.109

Beamforming maps of the three main configurations (baseline, seal and new seal) were also plotted to assess noise maps obtained at the spectra for the three selected

frequencies. Figure 8 shows the resulting beamforming maps for flyover measurements from a range between 5000 till 14000 Hz. Despite computed from 500 to 36000 Hz, they are not shown in all range since the large array beamwidth and the coherence loss affect the results for low and high frequencies, respectively. Most of the maps present a defined noise source, however, the apparently random shape of some maps with no consistent source means that no noise source is presented in the model region, presenting only side-lobes from other sources. This is related to higher decrease in the radiated noise for these specific configurations and frequencies.

The array of microphones identifies a strong noise source from the flap side-edge located at x/c ≈ 0.18 for baseline, seal and new seal configurations, which corresponds to the first part of the flap side-edge (leading-edge region) local flow-field noise described by Drobietz, R., and Borchers, I., (2006) [13]. In general, noise source maps clearly revealed the way the acoustical radiated noise decreased from low- to high-frequency spectra.

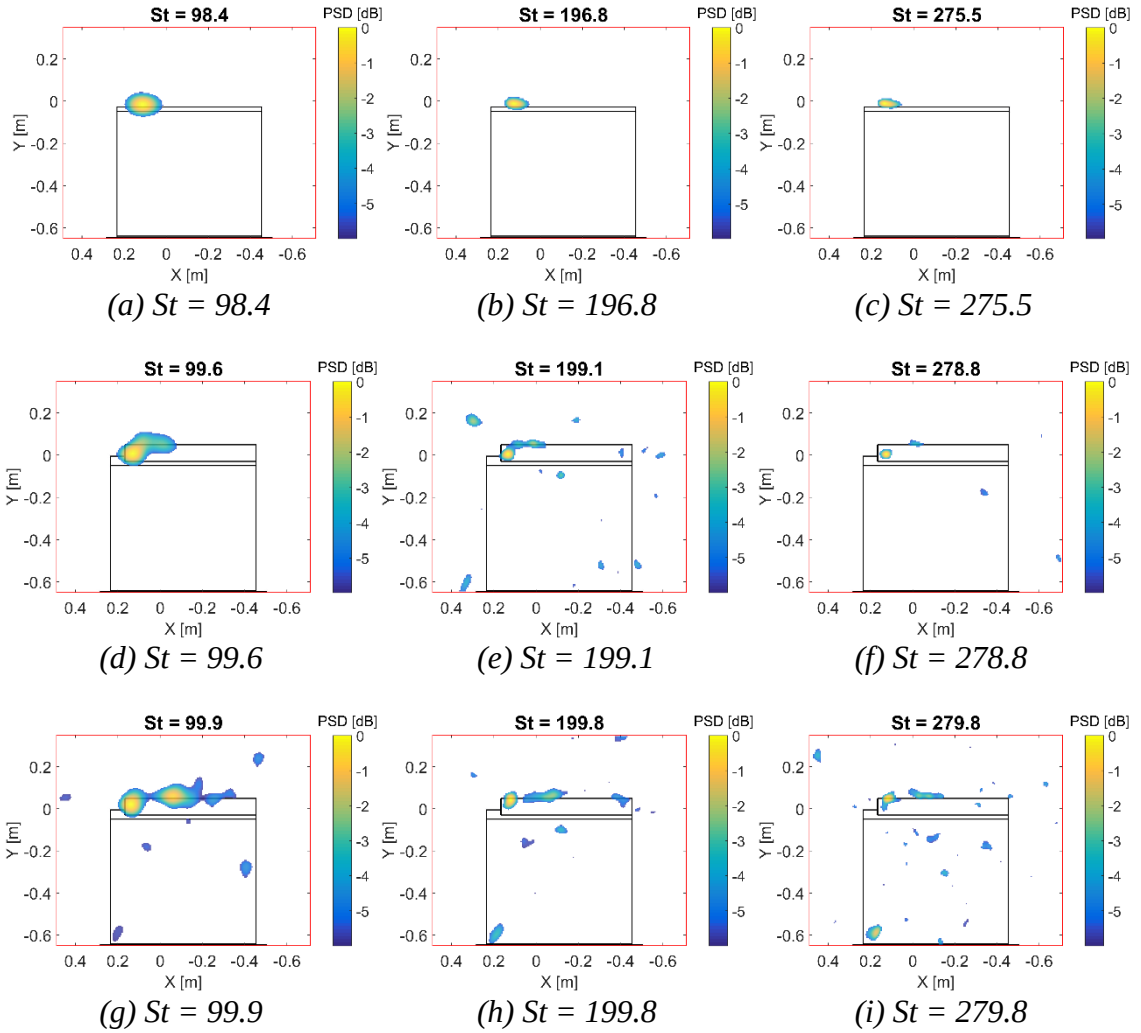

(a) St = 98.4 *(b) St = 196.8* *(c) St = 275.5*

(d) St = 99.6 *(e) St = 199.1* *(f) St = 278.8*

(g) St = 99.9 *(h) St = 199.8* *(i) St = 279.8*

Figure 8. Beamforming maps of noise source localization for flyover position obtained at $\alpha = 26^{o}$ and M = 0.109. Baseline flap side-edge (a-c), seal flap side-edge (d-f) and new seal flap side-edge (g-i). Black refers to the flap model and red denotes the integration region

The comparison in Figure 9 provides new understanding about the high broadband noise reduction achieved with the use of the tips in flyover case. Comparing the results for the three geometries tested, the seal and new seal side-edge tips, an important noise reduction in mid to high frequencies was perceived for flyover measurements. The tips

produced 3.9 and 6.1 dB less noise than the baseline flap side-edge, respectively as shown in Table 2. Additionally, the perforation was more productive for the seal flap side-edge with 6.7 dB (71 % less noisy than non-perforated tip) than for the new seal flap side-edge with 7.1 dB (16 % less noisy than non-perforated tip), however, the last configuration was the most efficient flap side-edge tip for noise reduction.

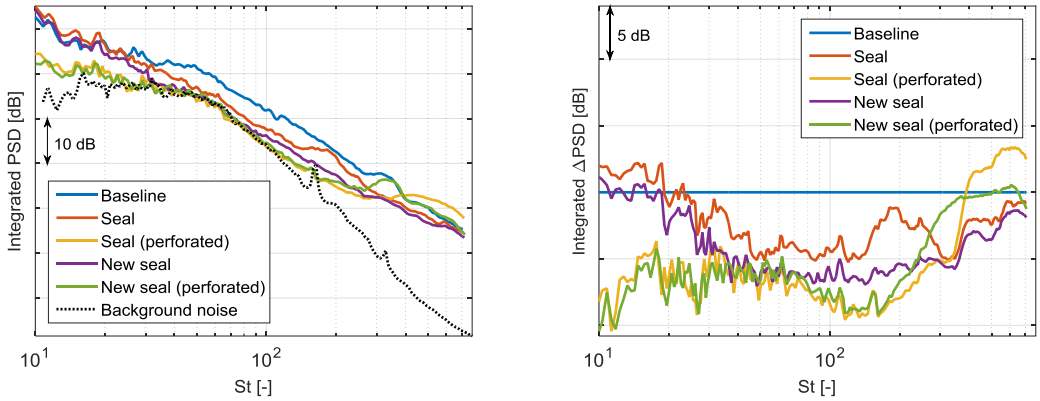

(a) Acoustic spectrum variation *(b) Acoustic spectrum of noise reduction*

Figure 9. Effect of the perforated flap side-edge tips on far-field noise spectrum at α = 26º

Table 2. Noise reduction measured for different perforated flap side-edge tips for flyover position at α = 26º and M = 0.109

Flap side-edge tip	Reduction [dB]
Baseline	0
Seal	3.9
Seal (perforated)	6.7
New seal	6.1
New seal (perforated)	7.1

Figure 10 depicts computational source directivity observed for the three main different tips at a parallel plane.

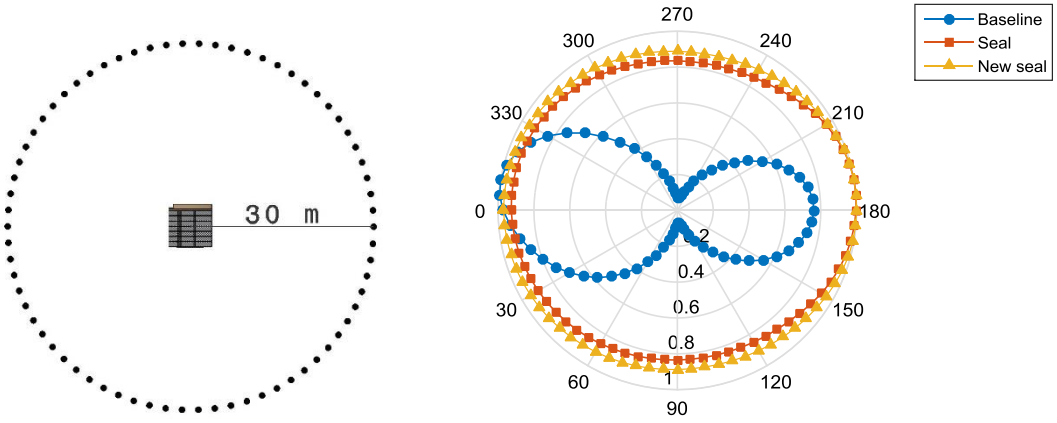

(a) Microphone directivity array *(b) Numerical noise directivity in a parallel plane*

Figure 10. Numerical noise directivity measured for flap side-edge tips at α = 26º and M = 0.109

As expected, baseline tip presents a dipole directivity and its noise is radiated more efficiently at angles closed to 0º and 180º following the leading- and trailing-edge, respectively. Directivity patterns for seal and new seal tips were similar with a monopole directivity propagation.

Directivity results are divided by the maximum value of each configurations, which produce and increment in noise radiation by the two quietest configurations in flyover measurements.

6. CONCLUSIONS

Detailed flow measurements were performed in a large-scale flap model in flyover position with three main different side-edge tips, in the LAE-1 wind tunnel at the São Carlos School of Engineering - University of São Paulo (EESC-USP) and the commercial software PowerFLOW 5.3 ®, for the experimental and numerical evaluation of the noise reduction from flap side-edge, respectively. The investigation determined the aeroacoustics of the flow-field around the flap side-edge for the understanding of the mechanisms responsible for the noise generation. A perforated material was applied to the flap side-edge in an attempt to reduce the noise. Flap acoustic noise was investigated by a phased array of microphones and beamforming techniques.

The far-field aeroacoustic predictions were compared for both the experimental and numerical analysis and revealed similar comparisons of noise spectrum between the experimentally measured beamforming results and the numerically obtained Ffowcs-Williams Hawkins results. According to the analysis of the filtered pressure spectrum, the spectrum results indicated the side-edge region exerts a strong influence on the total noise, which is in agreement with the quantitative beamforming source location maps that showed the main source of noise was located in the leading-edge region. The seal and new seal tips decrease acoustic noise in 3.9 and 6.1 dB in comparison with the baseline case. The effect of applying a perforated flap side-edge was most noticeable in reducing the low and mid frequency broadband noise. Perforated tips reduce the broadband noise in comparison with the baseline side-edge tip; perforated seal and new seal tips reduce 6.7 and 7.1 dB, respectively, of the overall sound pressure level of the flap model. In addition, large-scale perforated noise reduction devices are in agreement with the implementation of real-scale devices without the necessity of scaling perforations.

Finally, flap directivity patterns in a parallel plane follow the dipole model for baseline case with most of the energy propagating to the leading- and trailing-edge and monopole propagation for seal and new seal flap side-edge tips. The last two tips could increment noise radiation in sideline plane by their monopole characteristic.

7. ACKNOWLEDGEMENTS

The authors acknowledge the financial support from FINEP (Financiadora de Estudos e Projetos), CAPES (Coordenação de Aperfeiçoamento de Pessoal de Nível Superior) and CNPq (Conselho Nacional de Desenvolvimento Científico e Tecnológico).

8. REFERENCES

1. Smith, M. J., "*Aircraft noise*", Vol. 3, Cambridge University Press, (1989).

2. Crighton, D. G., "*Aeroacoustics of flight vehicles: Theory and practice. volume 1. noise sources*", NASA Langley Research Center, (1991).

3. Chow, L., Mau, K., and Remy, H., "*Landing gears and high lift devices airframe noise research*", 8th AIAA/CEAS Aeroacoustics Conference & Exhibit, (2002), p. 2408.

4. Airbus, "*Aircraft Noise - Technologies and Operations*", Tech. rep., Airbus, (2007).

5. Choudhari, M. M., Lockard, D. P., Macaraeg, M. G., Singer, B. A., Streett, C. L., Neubert, G. R., Stoker, R. W., Underbrink, J. R., Berkman, M. E., and Khorrami, M. R., "*Aeroacoustic experiments in the NASA Langley low-turbulence pressure tunnel*", (2002).

6. Dobrzynski, W., "*Almost 40 Years of Airframe Noise Research – What did we achieve?*", 14th Aeroacoustics Conference, (2008), p. 37.
7. Dobrzynski, W., "*Almost 40 years of airframe noise research: what did we achieve?*" Journal of aircraft, Vol. 47, No. 2, (2010), pp. 353–367.
8. Macaraeg, M. G., Lockard, D. P., and Streett, C. L., "*In search of the physics: NASA's approach to airframe noise*", (1999).
9. Rossignol, K.-S. S., "*Flow field measurements to characterize flap side-edge noise generation*", 19th AIAA/CEAS Aeroacoustics Conference, (2013), p. 2061.
10. Reichenberger, J., "*Noise Control on Flap Side Edge*", INTER-NOISE and NOISE-CON Congress and Conference Proceedings, Vol. 253, Institute of Noise Control Engineering, (2016), pp. 2424–2428.
11. Molin, N., Roger, M., and Barre, S., "*Prediction of aircraft high-lift device noise using dedicated analytical models*", 9th AIAA/CEAS Aeroacoustics Conference and Exhibit, (2003), p. 3225.
12. Filippone, A., "*Aircraft noise prediction*", Progress in Aerospace Sciences, Vol. 68, (2014), pp. 27–63.
13. Drobietz, R., and Borchers, I., "*Generic wind tunnel study on side edge noise*", 12th AIAA/CEAS Aeroacoustics Conference (27th AIAA Aeroacoustics Conference), (2006), p. 2509.
14. Acevedo, D., Botero, L., Lima Pereira, L. T., Catalano, F., Reis, D. C., and Coelho, E. L., *"Experimental Aeroacoustic and Aerodynamic Analysis of a Large-scale Flap Side-edge Model*", 2018 AIAA/CEAS Aeroacoustics Conference, (2018), p. 3799.
15. Catalano, F., "The New Closed Circuit Wind Tunnel of the Aircraft Laboratory of University of Sao Paulo, Brazil," 24th International Congress of the Aeronautical Sciencies ICAS, Yokohama, Japan, (2004).
16. Santana, L., Catalano, F. M., Medeiros, M. A., and Carmo, M., "*The update process and characterization of the Sao Paulo University wind-tunnel for aeroacoustics testing*", 27th International Congress of the Aeronautical Sciences ICAS, Nice, France, (2010).
17. Fonseca, W. D., Ristow, J. P., Sanches, D. G., and Gerges, S. N., "*A different approach to archimedean spiral equation in the development of a high frequency array*", Tech. rep., SAE Technical Paper, (2010).
18. Rion, C., "*NC-74 sound calibrator, data sheet*", (2003).
19. Allen, C. S., Blake, W. K., Dougherty, R. P., Lynch, D., Soderman, P. T., and Underbrink, J. R., "*Aeroacoustic measurements*", Springer Science & Business Media, (2013).
20. Sijtsma, P., "*CLEAN based on spatial source coherence*", International journal of aeroacoustics, Vol. 6, No. 4, (2007), pp.357–374.
21. Brooks, T. F., and Humphreys, W. M., "*Flap-edge aeroacoustic measurements and predictions*", Journal of Sound and Vibration, Vol. 261, No. 1, (2003), pp. 31–74.
22. Chen, S., and Doolen, G. D., "*Lattice Boltzmann method for fluid flows*", Annual review of fluid mechanics, Vol. 30, No. 1, (1998), pp. 329–364.2.
23. Santana, L. D., Carmo, M., Medeiros, M. A. F., and Catalano, F. M., "*The update of an aerodynamic wind-tunnel for aeroacoustics testing," Journal of Aerospace Technology and Management*, Vol. 6, No. 2, (2014), pp. 111–118.